Taylor & Francis
Taylor & Francis Group

Artificial Cells, Nanomedicine, and Biotechnology
An International Journal

ISSN: 2169-1401 (Print) 2169-141X (Online) Journal homepage: https://www.tandfonline.com/loi/ianb20

Development and characterization of a novel conductive polyaniline-g-polystyrene/Fe_3O_4 nanocomposite for the treatment of cancer

Lida Ahmadkhani, Ebrahim Mostafavi, Samaneh Ghasemali, Roghayeh Baghban, Hamidreza Pazoki-Toroudi, Soodabeh Davaran, Javad Malakootikhah, Nahideh Asadi, Lala Mammadova, Siamak Saghfi, Thomas J. Webster & Abolfazl Akbarzadeh

To cite this article: Lida Ahmadkhani, Ebrahim Mostafavi, Samaneh Ghasemali, Roghayeh Baghban, Hamidreza Pazoki-Toroudi, Soodabeh Davaran, Javad Malakootikhah, Nahideh Asadi, Lala Mammadova, Siamak Saghfi, Thomas J. Webster & Abolfazl Akbarzadeh (2019) Development and characterization of a novel conductive polyaniline-g-polystyrene/Fe_3O_4 nanocomposite for the treatment of cancer, Artificial Cells, Nanomedicine, and Biotechnology, 47:1, 873-881, DOI: 10.1080/21691401.2019.1575839

To link to this article: https://doi.org/10.1080/21691401.2019.1575839

ARTIFICIAL CELLS, NANOMEDICINE, AND BIOTECHNOLOGY
2019, VOL. 47, NO. 1, 873–881
https://doi.org/10.1080/21691401.2019.1575839

Development and characterization of a novel conductive polyaniline-g-polystyrene/Fe_3O_4 nanocomposite for the treatment of cancer

Lida Ahmadkhani[a,b], Ebrahim Mostafavi[c], Samaneh Ghasemali[d], Roghayeh Baghban[d], Hamidreza Pazoki-Toroudi[e], Soodabeh Davaran[a], Javad Malakootikhah[f], Nahideh Asadi[a], Lala Mammadova[g], Siamak Saghfi[g], Thomas J. Webster[c] and Abolfazl Akbarzadeh[b,h]

[a]Department of Medical Nanotechnology, Faculty of Advanced Medical Sciences, Tabriz University of Medical Sciences, Tabriz, Iran; [b]Tuberculosis and Lung Disease Research Center of Tabriz, Tabriz University of Medical Sciences, Tabriz, Iran; [c]Department of Chemical Engineering, Northeastern University, Boston, MA, USA; [d]Department of Medical Biotechnology, Faculty of Advanced Medical Science, Tabriz University of Medical Sciences, Tabriz, Iran; [e]Physiology Research Center and Department of Physiology, Iran University of Medical Sciences, Tehran, Iran; [f]Department of Life Science Engineering, Faculty of New Sciences & Technologies, University of Tehran, Tehran, Iran; [g]Department of Biophysics and Molecular Biology, Baku State University, Baku, Azerbaijan; [h]Universal Scientific Education and Research Network (USERN), Tabriz, Iran

ABSTRACT

The goal of this study is to synthesize, characterize and investigate some physicochemical properties of conductive polyaniline-g-polystyrene/Fe_3O_4 (Fe_3O_4/PSt-g-PANi) nanocomposites. For this purpose, initially, Fe_3O_4 nanoparticles were synthesized by a co-precipitation method. Then, the desired nanocomposite was synthesized in two steps. First, the atom transfer radical polymerization (ATRP) of styrene was performed using an ATRP initiator attached to the surface of Fe_3O_4 nanoparticles, followed by functionalization of the Fe_3O_4-PSt with amine groups (–NH_2). Second, surface oxidative graft copolymerization of aniline was accomplished using the –NH_2 moieties on the Fe_3O_4/PSt-NH_2 as the anchoring sites. The prepared materials were characterized by various instruments, including TEM, SEM, TGA, EDX, FT-IR, XRD and conductivity measurements. The results indicated that the synthesized conductive polymer/Fe_3O_4 nanocomposites had higher electrical conductivity and thermal resistance than those of the corresponding homopolymers.

ARTICLE HISTORY
Received 11 October 2018
Revised 18 December 2018
Accepted 19 December 2018

KEYWORDS
Graft copolymer; Fe_3O_4 nanoparticles; atom transfer radical polymerization; nanocomposite

Introduction

In recent decades, inorganic/organic composites have attracted the attention of scientists in both scientific and industrial fields. These composites possess unique properties (such as thermal stability) and have various functional groups within a single material. These composite/hybrid materials present novel and wonderful properties (e.g. mechanical, chemical, electrical, rheological, magnetic, optical, catalytic and so on). They have different applications in areas such as drug delivery systems, diagnostics, coatings and catalysis [1–10].

Conducting polymers (CPs) are significant because of their relatively easy processability, thermal and environmental stabilities and tunable electrical conductivities, for example, polyaniline (PANI) [11], polypyrrole (PPy) [12] and polythiophene (PTP) [13,14]. Conducting polymers may have potential applications in areas such as composite materials, tissue engineering, separation membranes, surface-activation materials, supercapacitor, electronic and electro-optic devices, as well as molecular motors [15–17]. Novel advances in polymer engineering have certainly increased the investigation of nanostructured CPs [18,19]. A new challenge in this area of nanotechnology is the capability to synthesize relatively small monodispersed CPs nanostructures, and their composites with metal oxide nanoparticles that have multifunctional properties [11,20–23].

Encapsulation of nanoparticles, such as metal oxides into conducting polymers, leads to nanohybrid organic/inorganic composites that demonstrate high thermal resistance, catalytic, electrochemical, optical, mechanical, electrical properties [24–27]. Also, metal oxide nanoparticles in conducting polymeric matrices allow for the development of products in many applications in sensors, microelectronics, cancer therapy, etc [28–31]. The unique properties of such compositions are essentially dependent on their size and shape. Diverse conducting polymer/inorganic particle composites have been synthesized by different methods and their properties and applications studied [32–37]. For example, Sadek et al. have reported In_2O_3–PANI composites as sensors for H_2, NO_2 and CO gases [33,38]. Xu et al. published the synthesis of a Pt–PANI composite and its application in detecting glucose [34]. De et al. studied TiO_2–PANI nanocomposites that can be used as electronic gadgets like capacitors [35]. V_2O_5–PANI composites have remarkable promise for their use as a

CONTACT Abolfazl Akbarzadeh akbarzadehab@tbzmed.ac.ir, dr.akbarzadeh2010@gmail.com Tuberculosis and Lung Disease Research Center of Tabriz, Tabriz University of Medical Sciences, Tabriz, Iran
This article has been republished with minor changes. These changes do not impact the academic content of the article.

cathode material for lithium secondary batteries [36]. One of the distinctive applications of polyaniline is its use in photothermal therapy of cancer. Xia et al. [39], Hong et al. [40] and Zhou et al. [20] have reported polyaniline as drug carriers for the photothermal therapy of cancer.

With the expansion of magnetic materials, significant research attempts have been created to synthesize conjugated polymers with magnetic materials to generate new magnetic and electrically conducting organic/inorganic materials, that can be used in electromagnetic interposition shielding, data storage and biomedical applications [41–49]. Different methods have been improved to make conducting magnetic nanocomposites, such as through the precipitation of iron salt in a polymer matrix [50,51], the *in situ* synthesis of the polymer by oxidative [52] or electrochemical [53] processes in the presence of well-dispersed magnetic nanoparticles and polymerization of the monomer [54–56].

A new method for the synthesis of organic/inorganic materials is controlled/living radical polymerization (CRP). CRP is a strong method for the synthesis of well-defined organic polymers because of a controlled molecular weight, narrow molecular weight distribution, combination and performance [57]. One of the methods of CRP is atom transfer polymerization (ATRP). ATRP has been commonly used for the preparation of polymers with a well-defined structure [58] by surface-initiated polymerization of various monomers, such as styrene, methacrylates, acrylates and dienes [59–63].

In the present study, we report a novel route for the synthesis of a brush polymer from the surface of Fe_3O_4 as core/shell nanoparticles. Therefore, we used the combination of two methods of ATRP of styrene and *in situ* chemical oxidation of aniline from the surfaces of the magnetic nanoparticles (Scheme 1). Characterization of this well-defined brush polymer has been investigated by performing FT-IR, thermogravimetric analysis, energy-dispersive X-ray (EDX), transmission electron microscopy (TEM), and X-ray diffraction (XRD). Considering the properties of the conductive polymer/Fe_3O_4 nanocomposite, it has potential applications in the treatment of cancer.

Experimental

Materials

Aniline and styrene monomers (Merck) were distilled under reduced pressure and stored below 0 °C. 2,2′-bipyridine (bpy), ammonium persulfate (APS), sulphuric acid, nitric acid, chloroform, $FeCl_3.6H_2O$, $FeCl_2.4H_2O$, NaOH, methanol and tin (II) chloride dihydrate were obtained from Merck. All chemicals were used as supplied without further purification. Copper chloride (I) (CuCl) (Merck) was stirred 12 h in acetic acid. Then, it was filtered, washed with absolute ethanol, and dried 24 h under a vacuum at 60 °C. 2-bromo-2-methyl propionic acid (Br-MPA) was obtained from Sigma Aldrich.

Preparation of the Fe_3O_4 nanoparticles

Fe_3O_4 nanoparticles were prepared using a co-precipitation path; it was synthesized without any additional stabilizer according to the following procedure. In summary, in this way, 0.79 M $FeCl_3.6H_2O$ and 0.4 M $FeCl_2.4H_2O$ were added to 25 ml of 0.4 M HCl. This solution of mixed iron salts was added dropwise to 250 ml of 1.5 M NaOH with stirring under an N_2 atmosphere. The obtained colloid solution was centrifuged at 5000 rpm, washed with an excess of deionized water and then dried in an oven for 6 h at 60 °C. A black fine powder (Fe_3O_4) was generated [64].

Preparation of an ATRP initiator onto Fe_3O_4 nanoparticles

2-bromo 2-methyl propionic acid (Br-MPA) (2.5 ml) and 1.5 g of Fe_3O_4 nanoparticles were dispersed in 50 ml methanol with the aid of ultrasound for 1 h. The dispersed solution was

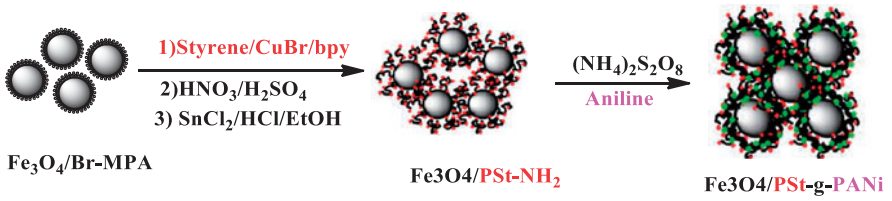

Scheme 1. Strategies for the preparation of well-defined and conductive polymer-Fe_3O_4 nanocomposites.

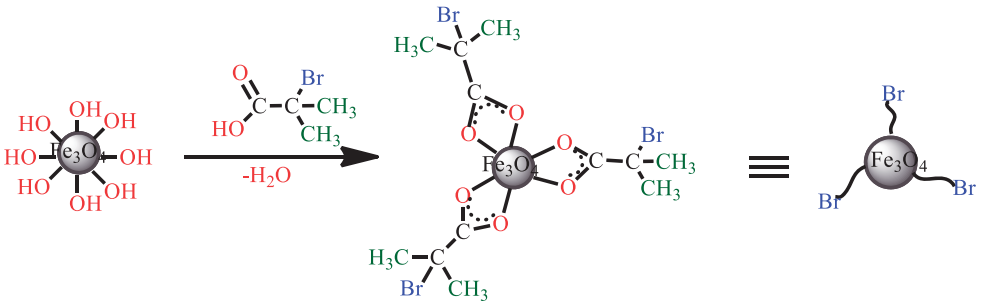

Scheme 2. Synthesis of ATRP initiator onto Fe_3O_4 nanoparticles.

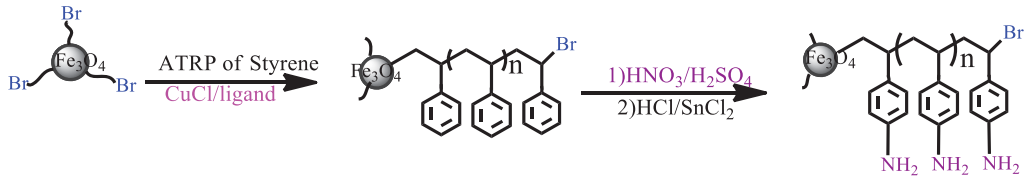

Scheme 3. Metal catalyzed controlled radical polymerization of styrene onto Fe_3O_4 nanoparticle and functionalization of grafted polymer.

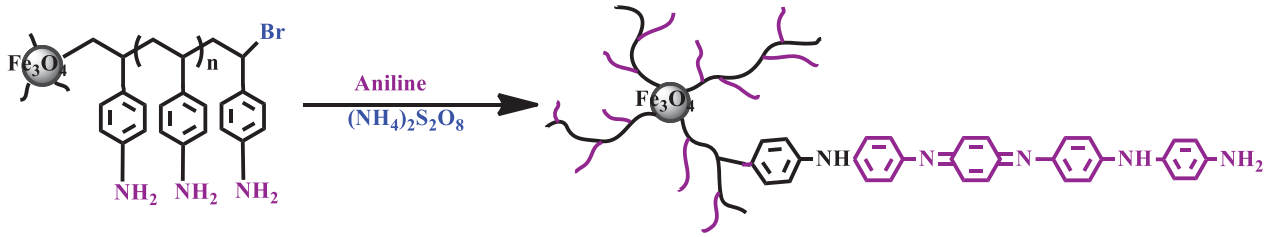

Scheme 4. Synthesis of conductive copolymer nanocomposite by *in situ* chemical oxidating polymerization.

then transferred to a 100 ml round bottom flask equipped with a condenser and a magnetic stirrer under nitrogen. The solution temperature was maintained at 65 °C under stirring for 24 h and then the solution was decanted and rinsed numerous times with methanol to remove non-chemisorbed Br-MPA; the solid product was dried overnight under vacuum at 60 °C (Scheme 2).

ATRP of styrene with Fe_3O_4/Br-MPA as the initiator

In the ATRP polymerization, functional nanoparticles with Br-MPA (25 mg) were mixed with a styrene monomer (2.5 ml). After purgation of the mixture with nitrogen for 10 min, it is transferred to a bottle with CuCl (4.9 mg) and 2,2′-bipyridine (19 mg). The reaction temperature was raised to 120 °C. After finishing the reaction time (20 h), the mixture was diluted with tetrahydrofuran (THF). The final products were precipitated with methanol. For further characterization, it was dissolved in toluene to form a clear yellowish solution [65] (Scheme 3).

Preparation of poly(p-amino styrene)-coated Fe_3O_4 (Fe_3O_4/PS-NH_2)

First, the nitroxide group is produced on polystyrene backbone using strong nitric acid and sulphuric acid. In a round-bottomed flask containing strong nitric acid(15 ml), which was placed in the ice-water bath, the polystyrene coated iron oxide nanoparticles (Fe_3O_4/PS) (0.75 gr) was suspended in it. Then, 23 ml of strong sulphuric acid was slowly added to it and the temperature was enhanced to 30 °C and continued for 10 h. After the desired time, the product was filtered and washed with sufficiently of water. It was transferred to a Soxhlet's extraction apparatus for reflux-extraction in 96% ethanol for 10 h. The product was dried under vacuum at 50 °C over 48 h. The product obtained in this step was Fe_3O_4/PS-NO_2 (Scheme 3).

Next, the nitroxide group was reduced to an amino group. In a round-bottomed flask containing 20 ml of hydrochloric acid (6M) and 23 ml of absolute ethanol, the Fe_3O_4/PS-NO_2 was suspended in it. Subsequently, 1.5 g of $SnCl_2.2H_2O$ was added to it, then, the temperature was enhanced to 75 °C and continued for 12 h. After the desired time, the product was washed with 10% NaOH solution, distilled water and absolute ethanol. To wash the Fe_3O_4/PS-NH_2, it was transferred to a Soxhlet's extraction apparatus for reflux-extraction in absolute ethanol for 10 h. The Fe_3O_4/PS-NH_2 obtained was dried under vacuum at 40 °C for 48 h (Scheme 3).

Preparation of Fe_3O_4/polystyrene-g- polyaniline, core/shell nanoparticles

For surface oxidative graft copolymerization of aniline is the same as in the Abbasian et al [65]. Briefly, the Fe_3O_4/PSt-NH_2 (0.1 g), aniline monomers (0.01 mol) were added into the aqueous solution of hydrochloric acid (1.0 M). The oxidant solution (2.6 mol of $(NH_4)_2S_2O_8$ in 20 ml of 1.0 M HCl) was added into the reaction mixture at 0 °C. The oxidative graft copolymerization was performed for 8 h. The PSt-NH_2 was used as the anchoring sites for polyaniline. The final product was dispersed into 1-methyl-2-pyrrolidone and centrifuged to remove the PANI homopolymer (Scheme 4).

Instrumentation

FT-IR spectra were recorded using a Shimadzu FT-IR-8101M; the spectrum was recorded at room temperature. The thermal properties of the Fe_3O_4/PSt-g-PANI nanocomposite measurement were determined by TGA-PL (England). XRD spectra were obtained using a Siemens D 5000 (Berlin, Germany), X-ray generator (CuK_α radiation with $\lambda = 1.5406$ Å) with a 2θ scan range of 2 to 80° at room temperature. The size and morphologies of the products were examined by scanning electron microscopy (SEM; Cam Scan MV 2300). The samples for SEM imaging were coated with a thin layer of gold film to avoid charging. Transmission electron microscopy (TEM) images were performed on a Philips EM208 microscope (Phillips, Eindhoven, Netherlands) with a 100 kV accelerating voltage. The conductivity of the samples was measured at room temperature by a standard four-probe apparatus (Azar Electric Co., Urmia, Iran). Electrochemical experiments were conducted using Auto-Lab PGSTA T302N.

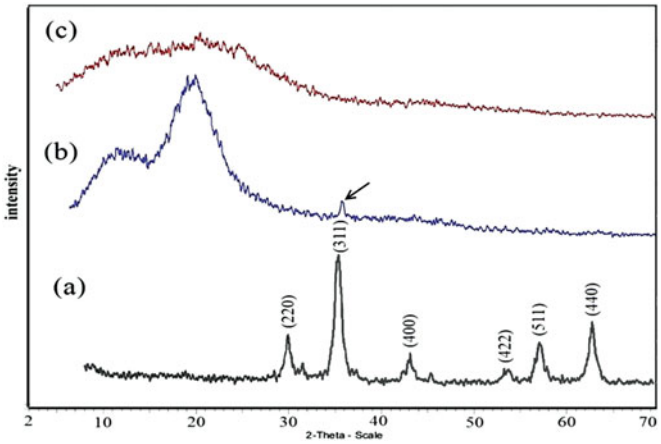

Figure 1. X-ray diffraction spectra of Fe_3O_4 nanoparticles (a) Fe_3O_4/PSt (b) Fe_3O_4/PSt-g-PANi.

Results and discussion

Preparation and surface modification of the magnetic nanoparticles

The Br-MPA attached to the surface of the iron oxide nanoparticles were used for ATRP polymerization. In addition, Br-MPA helps to stabilize nanoparticles in an organic solvent.

The XRD spectrum of Fe_3O_4 is displayed in Figure 1(a). The XRD spectrum indicated that the nanoparticles do not have any impurities. The average size of the Fe_3O_4 nanoparticles was calculated as ~11 nm using the Debye Sherrer's formula and the peak from 311 reflection [66].

$$D_c = k\lambda/b\ \cos\theta \tag{1}$$

The equation uses the reference peak width at angle θ, where λ is the X-ray wavelength (1.54060 Å), b is the width of the XRD peak at half height and k is a shape factor, about 0.89 for magnetite.

The atom transfer radical polymerization (ATRP) initiator, Br-MPA, was attached on the Fe_3O_4 nanoparticles through the esterification reaction. The evidence showed that Br-MPA was chemically bonded to Fe_3O_4 nanoparticles. The FT-IR spectrum of Fe_3O_4 (a), functional carboxylic acid (Br-MPA) (b), and Br-MPA -modified Fe_3O_4 (c) are shown in Figure 2. The FT-IR spectrum of the Fe_3O_4 nanoparticles was showed in Figure 2(a). The peak at 3417 cm^{-1} is related to the stretching vibrations of −OH or water molecules adsorbed onto the surface of the Fe_3O_4 nanoparticles, and the peak at 565 cm^{-1} is attributed to the stretching vibration mode of Fe–O. In Figure2(b), due to the structure of functional carboxylic acid (Br-MPA), there are characteristic adsorptions bands in the FT-IR spectrum. The peak at 2944–2843 cm^{-1} region is attributed to stretching vibration of C–H, the band around 1700 cm^{-1} is due to the stretching vibration of C=O, and the peak at 3008 cm^{-1} is ascribed to the stretching vibrations of the OH group.

The FT-IR spectrum of surface modification of the magnetic nanoparticles by Br-MPA was displayed in Figure 2(c). The bands at 1625 cm^{-1} is related to the C=O stretch in the carboxylic acid. It showed that the Br-MPA was attached to the Fe_3O_4 nanoparticles. Asymmetric and symmetric C=O vibrations of carboxylate groups was displayed the double peaks at 1571–1535 and 1443 cm^{-1}. Unreacted hydroxyl

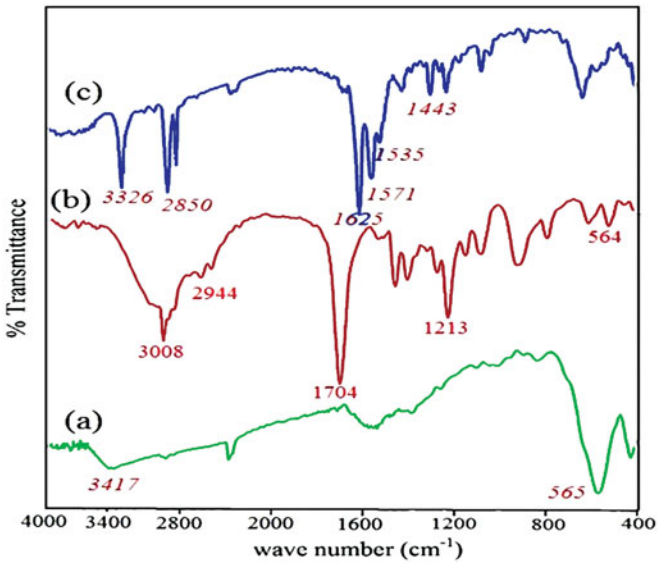

Figure 2. FT-IR spectra of (a) Fe_3O_4 nanoparticles (b) Br-MPA and (c) Fe_3O_4/Br-MPA.

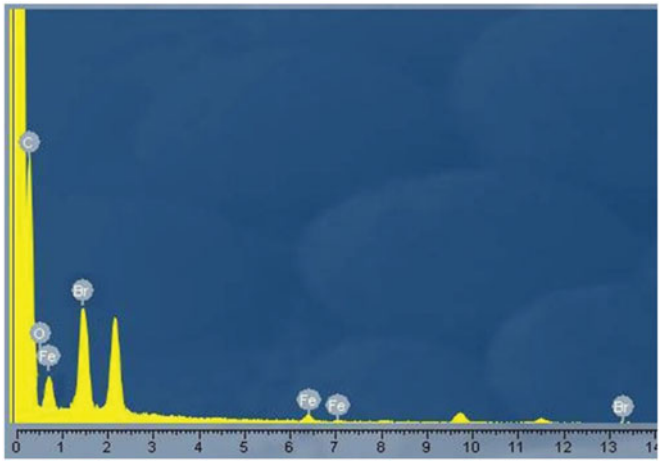

Figure 3. Energy-dispersive X-ray(EDX) analysis of Fe_3O_4/Br-MPA.

groups (–OH) on the nanoparticle surface appeared in 3326 cm^{-1}. The strong band at 2925 cm^{-1} (asymmetric) and 2850 cm^{-1} (symmetric) is related to the $-CH_2$ stretching vibrations.

Figure 3 and Table 1 showed the energy-dispersive X-ray (EDX) analysis spectrum of Fe_3O_4–Br–MPA. The presence of C, O, Fe and Br signals presented that the nanoparticle surfaces were modified by 2-bromo2-methyl propionic acid (Br–MPA).

ATRP polymerization of styrene with modified Fe_3O_4 nanoparticles

One of the preferences of ATRP [67,68] is that an alkene monomer like styrene can be polymerized with molecular weight and PDI control, either in bulk or in solution [69]. FT-IR, SEM and XRD can prove that the "grafting from" reaction proceeds successfully.

Figure 4(a) shows the FT-IR spectrum of Fe_3O_4/PSt. According to the FT-IR spectrum the characteristic absorption bands for polystyrene are as follows: the C–H aromatic stretching vibration at 3026 cm^{-1}, the C–H aliphatic stretching

Table 1. Energy-dispersive X-ray (EDX) analysis of Fe_3O_4-Br-MPA macroinitiator.

Element	Weight %	Atomic %
C K	46.43	73.09
O K	11.57	11.74
Fe K	8.47	7.59
Br K	33.53	7.58
Totals	100	–

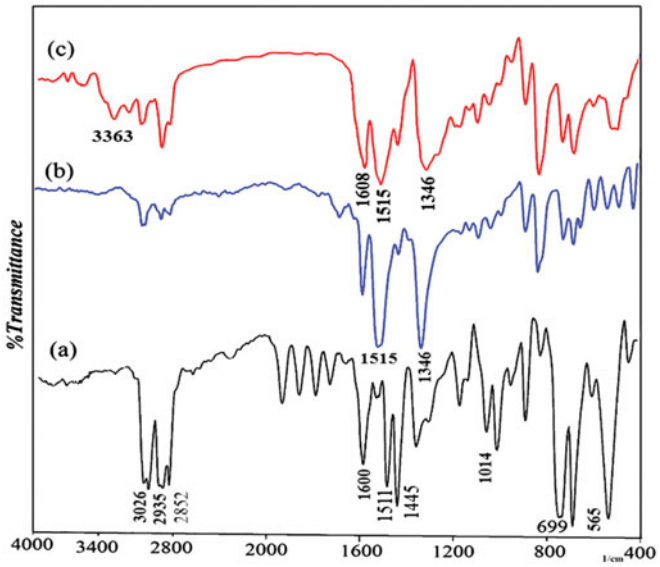

Figure 4. FT-IR spectra of (a) Fe_3O_4/PSt (b) Fe_3O_4/PSt-NO2 (c) Fe_3O_4/PSt-NH_2.

vibration at 2935 and 2852 cm^{-1}, the phenyl ring stretching vibration at 1445, 1511, the ring in phase C–H stretching vibration at 1014 cm^{-1}, and 1600 cm^{-1} corresponding to the C=C stretching of the aromatic ring and the ring out-of-plane bend at 699 cm^{-1}. The FT-IR spectrum of Fe_3O_4/PSt established with the PSt standard.

The morphology of the Fe_3O_4 nanoparticles and Fe_3O_4/PSt were probed using SEM. As shown in Figure 5(a), the Fe_3O_4 nanoparticles are spherical in shape with about 30 nm diameter. With the growth of the polystyrene chain on the Fe_3O_4 surface using initiators of ATRP polymerization, Br-MPA attached to Fe_3O_4 nanoparticles, larger particles were obtained (Figure 5(b)). Therefore, the Fe_3O_4 nanoparticle was coated with polystyrene and becomes core/shell nanocomposite. These materials with chemically bonds between organic and inorganic have improved properties.

Figure 1(b) shows the X-ray diffraction pattern after growth of polystyrene on the Fe_3O_4 nanoparticles. The appearance of peaks at $2\theta = 10$–$24°$ is related to polystyrene. This shows that the polystyrene has an amorphous structure. The characteristic peak at $2\theta = 35.5°$ is attributed to the presence of Fe_3O_4 nanoparticles.

Preparation of poly(p-amino styrene) grafted onto Fe_3O_4

FT-IR spectrum confirmed the structural characteristics of the obtained polymer-coated Fe_3O_4. In the spectrum line of Fe_3O_4-PS-NO_2, the absorption bands at 1515 cm^{-1} and 1346 cm^{-1} were attributed to the $-NO_2$ group (Figure 4(b)),

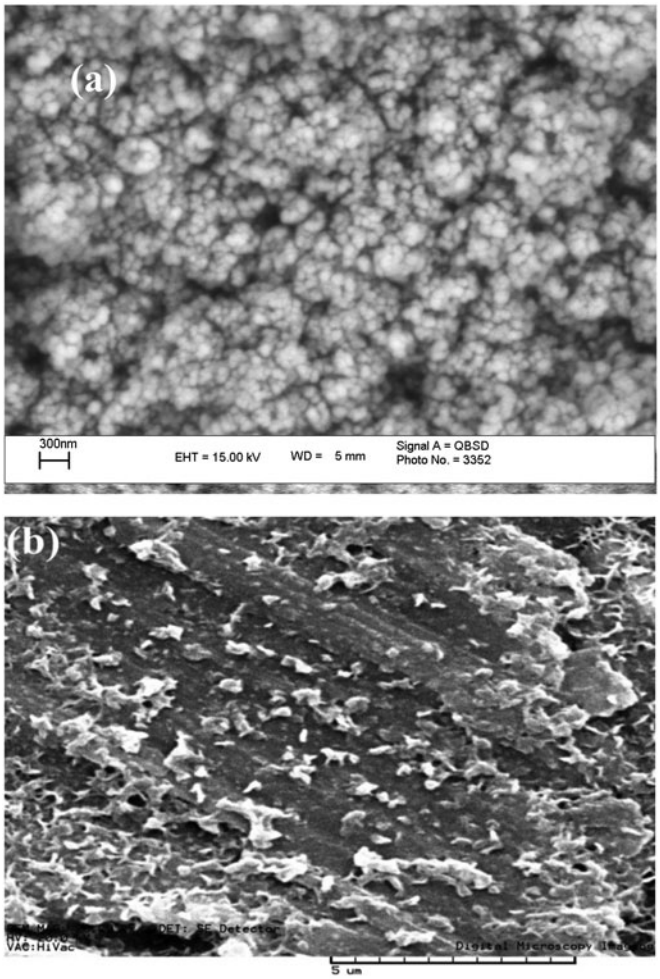

Figure 5. SEM image Of (a) Fe_3O_4 (b) Fe_3O_4/PSt.

which, suggested that the nitration reaction occurred and $-NO_2$ groups were attached to a benzene ring. After a reduction reaction and the production of amino groups, the bands at 3363 cm^{-1} and 1608 cm^{-1} became stronger because of the stretching vibration of N–H as shown in the FT-IR spectra of Fe_3O_4/PSt-NH_2 (Figure 4c). Furthermore, we found that the characteristic bands of $-NO_2$ at 1515 and 1346 cm^{-1} apparently became weaker, suggesting that $-NO_2$ groups were reduced to $-NH_2$.

Characterization of Fe_3O_4/polystyrene-g-polyaniline nanocomposites

The Fe_3O_4/polystyrene-g-polyaniline nanocomposite was characterized by FT-IR. Figure 6 shows the FT-IR spectrum of Fe_3O_4/polystyrene-g-polyaniline. The formation of polyaniline was shown by an absorption band at 3379 cm^{-1} which can be attributed to the N–H stretching mode; 1587, 1500 cm^{-1} is related to the C=N stretching mode for quinoid and C=C stretching mode for benzenoid units; and 1303, 1168 cm^{-1} can be attributed to the C–N stretching mode for the benzenoid unit. 1118 and 825 cm^{-1} can be attributed to the C–H in the benzene plane.

Figure1(c) displays the X-ray diffraction pattern for the Fe_3O_4/PSt-g-PANI nanocomposite. This is characterized by the

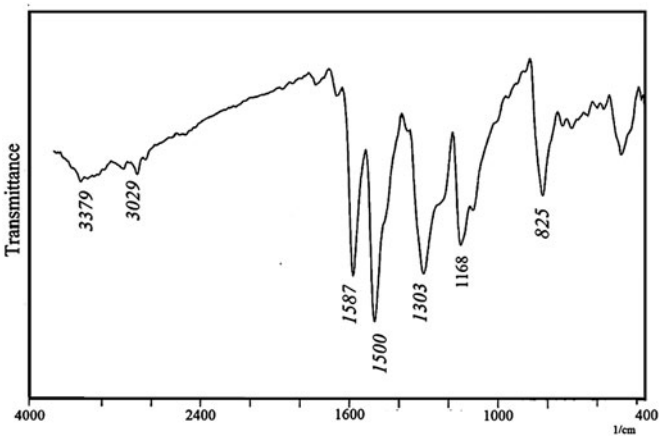

Figure 6. FT-IR spectra of Fe_3O_4/PSt-g-PANi nanocomposite.

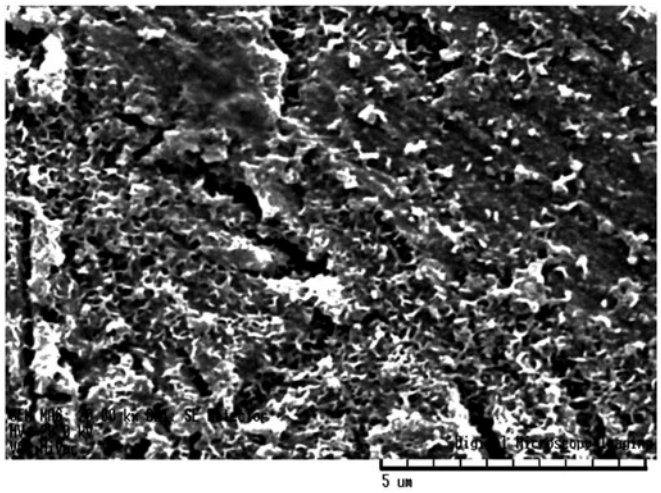

Figure 7. SEM of Fe_3O_4/PSt-g-PANi nanocomposite.

appearance of peaks extending over the 2θ range of 5° to 30°. This shows that the polymer has an amorphous structure and is a completely coated nanoparticle.

SEM was used to study the morphology of Fe_3O_4/PSt-g-PANI as shown in Figure 7. Much larger particles were obtained when the polymer chains grew from the Fe_3O_4/PSt surface (Figure 5(b)). The compacted and large amounts of polyaniline chains "clothe" the Fe_3O_4/PSt nanocomposite to become bulk materials.

Figure 8 shows the thermal behavior and thermogravimetric analysis (TGA) of the Fe_3O_4, Fe_3O_4/PSt and Fe_3O_4/PSt-g-PANI nanoparticles. As shown in Figure 8(a), the Fe_3O_4 nanoparticles exhibit high stability in the range of 50–800 °C. These nanoparticles have lost about 6% of their total weight. Probably the evaporation of absorbed water on the surface of nanoparticles had led to weight loss. Figure 8(b) is related to PSt-grafted Fe_3O_4 that shows a sharp weight loss (61%) at 300–350 °C. This weight loss is attributed to evaporation of solvent trapped between the polymer chains and the burning-up of the grafted polystyrene.

Figure 8(c) shows the thermal behavior of Fe_3O_4/PSt-g-PANI nanocomposite, i.e. 41% weight loss at 50–800 °C. The initial weight loss is about 3.6% at 127 °C that can be assigned to the decomposition of solvent molecules trapped between the polymer chains. The rapid weight decrease is in

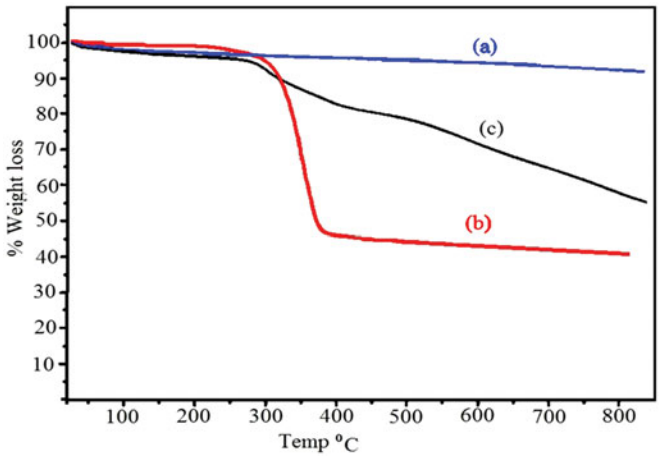

Figure 8. Thermogravimetric analysis of (a) Fe_3O_4 nanoparticles, (b) Fe_3O_4/PSt, (c) Fe_3O_4/PSt-g-PANi nanocomposite.

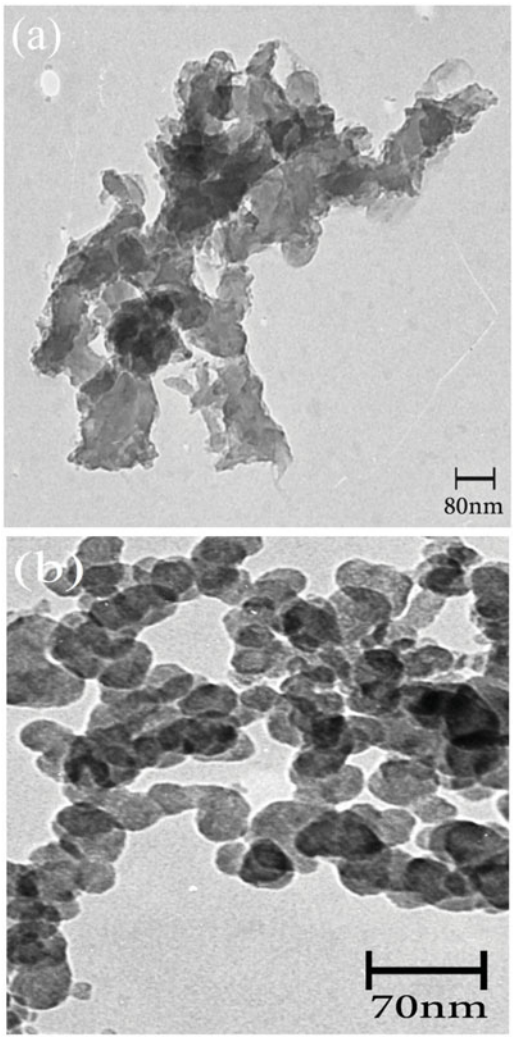

Figure 9. Transmission electron microscopy (TEM) images of (a) Fe_3O_4 nanoparticles (b) Fe_3O_4/PSt-g-PANi nanocomposite.

the second region at ~340 °C, which is attributed to the decomposition of homo-PANI. Moderate rate of weight loss in Fe_3O_4/PS-g-PANI could be related to the presence of the polyaniline chain on the backbone of polystyrene.

Figure 9(a) shows the TEM image of the Fe_3O_4 nanoparticles. The TEM image determines the size distribution and

morphology of the Fe_3O_4 nanoparticles. The Fe_3O_4 nanoparticles show high aggregation due to the large specific surface area. The TEM image in Figure 9(b) shows the Fe_3O_4/PSt-g-PANI nanocomposite. This image illustrated that aggregation and the dispersion were decreased and improved, respectively. The Fe_3O_4/PSt-g-PANI nanocomposite exhibited very good dispersion in the solvent.

Conductivity measurements

The electrical conductivity of polyaniline and its composites makes it suitable for electrical applications. Conductivity measurements were carried out by a four-point probe method. The blends of PANI nanocomposites were compacted into pellets for measurement. All measurements were done in air at room temperature and converted to conductivity by the following equation:

$$\rho = 1/\delta = V/I\omega\pi/\ln 2 \quad (2)$$

In this equation, ρ is the resistivity (Ω cm), δ is the conductivity (s/cm), V is the potential difference (mV), I is the applied constant current (mA), and ω is the thickness (cm). The conductivity of the nanocomposite was high compared to that of PANI. The improved conductivity of the composite is possibly due to the charge transfer between Fe_3O_4 nanoparticles and PANI. The conductivity values of the pure PANI and its nanocomposites were 1.32 and 1.25 Scm^{-1}, respectively (Table 2).

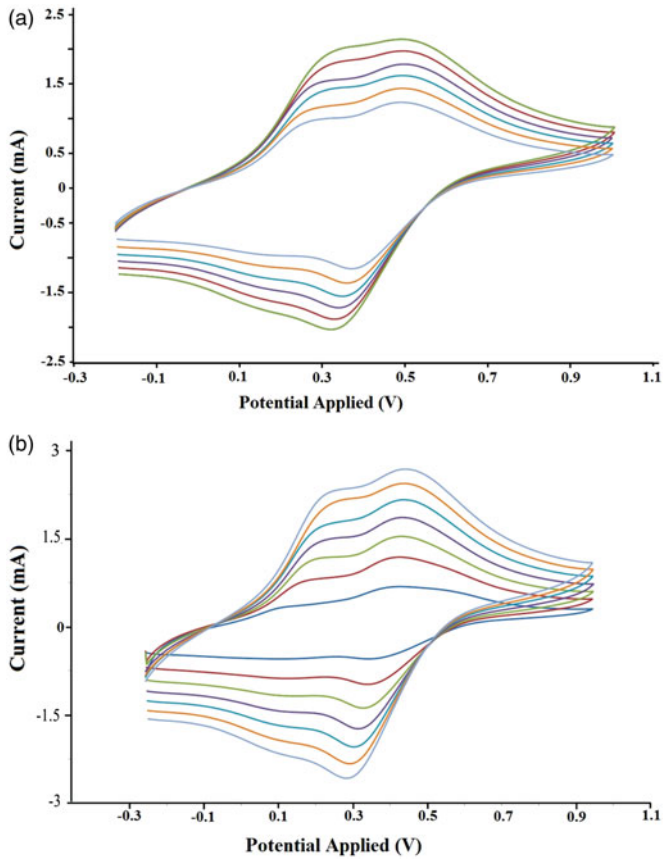

Figure 10. Cyclic voltammetry curves (CVs) of the chemically synthesized (a) homo-PANi (b) Fe_3O_4/PSt-g-PANi.

As shown in Figure 10, the effect of the potential scanning rate (V) on the peak currents for the chemically synthesized homo and nanocomposite of PANi were investigated under cyclic voltammetric (CV) conditions in the range of 10 to 90 mVs^{-1}, in DMSO between −0.20 and +1.00 V. All potentials are given versus the reference (Ag/AgCl) electrode. The polymer film was prepared on glassy carbon (GC) microelectrode by casting the polymeric solution of samples in THF by ultrasonic treatment for 10 min.

Typical cyclic voltammograms (CVs) of the homoPANI film are shown in Figure 10(a). As seen, the CVs of the homoPANI indicated two anodic peaks at around 0.31 and 0.52 V versus the reference electrode. Moreover, as can be realized, the anodic peaks shifted in the direction of a positive potential with increasing scan rate, which indicated that the electrochemical doping/dedoping of the casted polymer film was chemically reversible. In Figure 10(b), the CVs of the nanocomposite of the PANI film exhibited two typical redox couples with anodic peaks at about 0.26 and 0.47 V against the Ag/AgCl electrode. A similar voltammogram of pure polyaniline for the nanocomposites of PANi showed that the anodic peaks currents linearly increased with increasing scan rate. Also, Figure 10(b) shows that despite the polystyrene chains, the PANI nanocomposite is electrically conductive.

Conclusion

A Fe_3O_4/PSt-g-PANi nanocomposite was successfully synthesized with a core-shell structure and a new path, combining surface-initiated atom transfer radical polymerization of styrene with pattern-guided oxidative polymerization of aniline. Immobilization of an ATRP initiator on the Fe_3O_4 surface allowed for the subsequent surface-initiated ATRP to produce polystyrene grafted polymers. Then, functionalization of the polystyrene grafted to the amino group was completed. The resulting macroinitiator (Fe_3O_4/PSt-NH_2) was used for in-situ chemical oxidating of aniline. FT-IR and TGA data verify that the surface modification of Fe_3O_4 by a chemical grafting approach was indeed successful. FT-IR, XRD, TGA, TEM, and SEM confirmed the success of the synthesis and polymerization processes. The synthesized Fe_3O_4/polystyrene-g-polyaniline showed better electrical conductivity and better thermal stability relative to homopolymers. Moreover, morphological studies by SEM and TEM presented direct and clear evidence for grafting of polystyrene and polyaniline to the Fe_3O_4 surface nanoparticles. The method presented for the preparation of the Fe_3O_4/polymer nanocomposite is attractive because the chemical grafting of the polymers to Fe_3O_4 has benefits over a composite prepared by the simple mixing of components.

Table 2. Characteristics of the conductive nanocomposite.

sample	Polymerization time(h)	Particle size (nm)	Shell thickness (nm)	Conductivity (σ(S/cm))
Fe_3O_4	–	10–21	–	–
Fe_3O_4/PSt-g-PANi	8	12–50	7–14	1.32

Due to improved physicochemical properties relative to the homopolymers, the synthesized nanocomposite could be beneficial for numerous applications from supercapacitors or other electronic devices to medicine. This nanocomposite showed high electrical conductivity of about 1.25 Scm^{-1}.

Disclosure statement

No potential conflict of interest was reported by the authors.

ORCID

Ebrahim Mostafavi http://orcid.org/0000-0003-3958-5002

References

[1] Zhu J, Morgan AB, Lamelas FJ, et al. Fire properties of polystyrene-clay nanocomposites. Chem Mater. 2001;13:3774–3780.
[2] Caruso F, Spasova M, Susha A, et al. Magnetic nanocomposite particles and hollow spheres constructed by a sequential layering approach. Chem Mater. 2001;13:109–116.
[3] Cho JD, Ju HT, Hong JW. Photocuring kinetics of UV-initiated free-radical photopolymerizations with and without silica nanoparticles. J Polym Sci A Polym Chem. 2005;43:658–670.
[4] Zhou J, Zhang S, Qiao X, et al. Synthesis of SiO2/poly (styrene-co-butyl acrylate) nanocomposite microspheres via miniemulsion polymerization. J Polym Sci A Polym Chem. 2006;44:3202–3209.
[5] Luo J, Wang X, Li J, et al. Conductive hybrid film from polyaniline and polyurethane–silica. Polymer 2007;48:4368–4374.
[6] Fleming MS, Mandal TK, Walt DR. Nanosphere-microsphere assembly: methods for core-shell materials preparation. Chem Mater. 2001;13:2210–2216.
[7] Moghimi SM, Hunter AC, Murray JC. Long-circulating and target-specific nanoparticles: theory to practice. Pharmacol Rev. 2001;53: 283–318.
[8] Mostafavi E, Soltantabar P, Webster TJ. Nanotechnology and picotechnology: A new arena for translational medicine. In: Biomaterials in translational medicine. Academic Press; 2019. p. 191–212.
[9] Rahmani Del Bakhshayesh A, Mostafavi E, Alizadeh E, et al. fabrication of three-dimensional scaffolds based on nano-biomimetic collagen hybrid constructs for skin tissue engineering. ACS Omega. 2018;3:8605–8611.
[10] Gharegozloo S, Ataie A, Abdizadeh H, et al. High performance Ni–CNTs catalyst: synthesis and characterization. RSC Adv. 2016;6: 47072–47082.
[11] Daikh S, et al. Chemical polymerization, characterization and electrochemical studies of PANI/ZnO doped with hydrochloric acid and/or zinc chloride: Differences between the synthesized nanocomposites. J Phy Chem Sol. 2018;121:78–84.
[12] Yamani K, et al. Preparation of polypyrrole (PPy)-derived polymer/ZrO 2 nanocomposites. J Ther Anal Calori. 1–12.
[13] MacDiarmid AG. "Synthetic metals": a novel role for organic polymers (Nobel lecture). Angew Chem Int Ed. 2001;40:2581–2590.
[14] Skotheim TA. Handbook of conducting polymers.: CRC press; 1997.
[15] Gök A, Sarı B, Talu M. Synthesis and characterization of conducting substituted polyanilines. Synthetic Metals. 2004;142:41–48.
[16] Wessling B. Progress in science and technology of polyaniline and poly-ethylenedioxythiophene. Synthetic Metals. 2003;135:265–268.
[17] Davaran S, Rashidi MR, Khandaghi R, et al. Development of a novel prolonged-release nicotine transdermal patch. Pharmacol Res. 2005;51:233–237.
[18] Mallick K, Witcomb MJ, Dinsmore A, et al. Fabrication of a metal nanoparticles and polymer nanofibers composite material by an *in situ* chemical synthetic route. Langmuir 2005;21:7964–7967.
[19] Huang L, Wang Z, Wang H, et al. Polyaniline nanowires by electropolymerization from liquid crystalline phases. J Mater Chem. 2002;12:388–391.
[20] Zhou J, Lu Z, Zhu X, et al. NIR photothermal therapy using polyaniline nanoparticles. Biomaterials. 2013;34:9584–9592.
[21] Benykhlef S, Bekhoukh A, Berenguer R, et al. PANI-derived polymer/Al2O3 nanocomposites: synthesis, characterization, and electrochemical studies. Colloid Polym Sci. 2016;294:1877–1885.
[22] Ahmadzadeh M, Ataie A, Mostafavi E. The effects of mechanical activation energy on the solid-state synthesis process of BiFeO 3. J Alloys and Comp. 2015;622:548–556.
[23] Mostafavi E, Babaei A, Ataie A. La0.6Sr0.4Co0.2Fe0.8O3 perovskite cathode for intermediate temperature solid oxide fuel cells: a comparative study. Iranian Journal of Hydrogen & Fuel Cell 2015; 1:239–246.
[24] Reddy KR, Lee K-P, Lee Y, et al. Facile synthesis of conducting polymer–metal hybrid nanocomposite by *in situ* chemical oxidative polymerization with negatively charged metal nanoparticles. Mater Lett. 2008;62:1815–1818.
[25] Choi M, Jang J. Heavy metal ion adsorption onto polypyrrole-impregnated porous carbon. J Colloid Interface Sci. 2008;325: 287–289.
[26] Reddy KR, Lee K-P, Gopalan AI, et al. Synthesis of metal (Fe or Pd)/alloy (Fe–Pd)-nanoparticles-embedded multiwall carbon nanotube/sulfonated polyaniline composites by γ irradiation. J Polym Sci A Polym Chem. 2006;44:3355–3364.
[27] Reddy KR, Lee K-P, Kim JY, et al. Self-assembly and graft polymerization route to monodispersed Fe3O4@ SiO2—polyaniline core–shell composite nanoparticles: physical properties. J Nanosci Nanotech. 2008;8:5632–5639.
[28] Asadi N, et al. Synthesis, characterization and *in vitro* evaluation of magnetic nanoparticles modified with PCL–PEG–PCL for controlled delivery of 5FU. Art Cells, Nanomed, and Biotechnol. 2018; 2018:1–8.
[29] Davaran S, Ghamkhari A, Alizadeh E, et al. Novel dual stimuli-responsive ABC triblock copolymer: RAFT synthesis,"schizophrenic" micellization, and its performance as an anticancer drug delivery nanosystem. J Colloid Interface Sci. 2017;488:282–293.
[30] Vahed SZ, et al. Liposome-based drug co-delivery systems in cancer cells. Mater Sci Eng: C. 2017;71:1327–1341.
[31] Davaran S, Entezami A. Synthesis and hydrolysis of polyurethanes containing ibuprofen pendent groups. J Bioact Compat Polym. 1997;12:47–58.
[32] Parvatikar N, Jain S, Khasim S, et al. Electrical and humidity sensing properties of polyaniline/WO 3 composites. Sens Actuat B: Chem. 2006;114:599–603.
[33] Sadek AZ, Wlodarski W, Shin K, et al. A layered surface acoustic wave gas sensor based on a polyaniline/In2O3 nanofibre composite. Nanotechnol. 2006;17:4488.
[34] Xu L, Zhu Y, Tang L, et al. Dendrimer-encapsulated Pt nanoparticles/polyaniline nanofibers for glucose detection. J Appl Polym Sci. 2008;109:1802–1807.
[35] Dey A, De S, De A, et al. Characterization and dielectric properties of polyaniline–TiO2 nanocomposites. Nanotechnol. 2004;15:1277.
[36] Huguenin F, Ferreira M, Zucolotto V, et al. Molecular-level manipulation of V2O5/polyaniline layer-by-layer films to control electrochromogenic and electrochemical properties. Chem Mater. 2004;16:2293–2299.
[37] Ajami M, et al. Effect of DHA + EPA on oxidative stress and apoptosis induced by ischemia-reperfusion in rat kidneys. Fundam Clin Pharmacol. 2013;27:593–602.
[38] Mostafavi E, Ataie A. Destructive interactions between pore forming agents and matrix phase during the fabrication process of porous BiFeO 3 ceramics. J Mater Sci Technol. 2015;31:798–805.
[39] Xia B, Wang B, Shi J, et al. Photothermal and biodegradable polyaniline/porous silicon hybrid nanocomposites as drug carriers for

combined chemo-photothermal therapy of cancer. Acta Biomaterialia. 2017;51:197–208.
[40] Hong Y, et al. Photothermal ablation of cancer cells using self-doped polyaniline nanoparticles. Nanotechnology. 2016;27: 185104.
[41] Gass J, Poddar P, Almand J, et al. Superparamagnetic polymer nanocomposites with uniform Fe3O4 nanoparticle dispersions. Adv Funct Mater. 2006;16:71–75.
[42] Wuang SC, Neoh KG, Kang E-T, et al. Synthesis and functionalization of polypyrrole-Fe 3 O 4 nanoparticles for applications in biomedicine. J Mater Chem. 2007;17:3354–3362.
[43] Sezavar H, Saboor-Yaraghi A-A, Salehi E, et al. Whether vitamin A supplementation is effective in T-bet and IFN-ɤ gene expression reduction? Immunol Investig. 2015;44:189–198.
[44] Mostafavi E, Ataie A, Ahmadzadeh M, et al. Synthesis of nanostructured Bi1− xBaxFeO3 ceramics with enhanced magnetic and electrical properties. Mater Chem Phys. 2015;162:106–112.
[45] Mostafavi E, Ataie A, Ahmadzadeh M. Characterization of nanostructured multiferroic bismuth ferrite produced via solid state reaction route. Amr. 2013;829:683–687.
[46] Ebrahimi E, Akbarzadeh A, Abbasi E, et al. Novel drug delivery system based on doxorubicin-encapsulated magnetic nanoparticles modified with PLGA-PEG1000 copolymer. Art Cells, Nanomed, and Biotechnol. 2016;44:290–297.
[47] Pazoki-Toroudi H, Nassiri-Kashani M, Tabatabaie H, et al. Combination of azelaic acid 5% and erythromycin 2% in the treatment of acne vulgaris. J Dermatolog Treat. 2010;21:212–216.
[48] Pazoki-Toroudi HR, et al. The preventive effect of captopril or enalapril on reperfusion injury of the kidney of rats is independent of angiotensin II AT1 receptors. Fund Clin Pharmacol. 2003;17: 595–598.
[49] Pazoki-Toroudi HR, Ajami M, Habibey R. Pre-medication and renal pre-conditioning: a role for alprazolam, atropine, morphine and promethazine. Fund Clin Pharmacol. 2010;24:189–198.
[50] Wan M, Zhou W, Li J. Composite of polyaniline containing iron oxides with nanometer size. Synthetic Metals. 1996;78:27–31.
[51] Mostafavi E, Babaei A, Ataie A. Synthesis of nano-structured La0. 6Sr0. 4Co0. 2Fe0. 8O3 Perovskite by co-precipitation method. J Ultrafine Grained and Nanostruct Mater. 2015;48:45–52.
[52] Deng J, Peng Y, He C, et al. Magnetic and conducting Fe3O4–polypyrrole nanoparticles with core-shell structure. Polym Int. 2003;52:1182–1187.
[53] Bidan G, Jarjayes O, Fruchart JM, et al. New nanocomposites based on "tailor dressed" magnetic particles in a polypyrrole matrix. Adv Mater. 1994;6:152–155.
[54] Suri K, Annapoorni S, Tandon RP, et al. Nanocomposite of polypyrrole-iron oxide by simultaneous gelation and polymerization. Synthetic Metals. 2002;126:137–142.
[55] Ebrahiminezhad A, Rasoul-Amini S, Kouhpayeh A, et al. Impacts of amine functionalized iron oxide nanoparticles on HepG2 cell line. Cnano. 2015;11:113–119.
[56] Pazoki-Toroudi H, Nilforoushzadeh MA, Ajami M, et al. Combination of azelaic acid 5% and clindamycin 2% for the treatment of acne vulgaris. Cutan Ocul Toxicol. 2011;30:286–291.
[57] Pyun J, Matyjaszewski K. Synthesis of nanocomposite organic/inorganic hybrid materials using controlled/"living" radical polymerization. Chem Mater. 2001;13:3436–3448.
[58] Matyjaszewski K, Qin S, Boyce JR, et al. Effect of initiation conditions on the uniformity of three-arm star molecular brushes. Macromolecules. 2003;36:1843–1849.
[59] Motornov M, Sheparovych R, Lupitskyy R, et al. Stimuli-responsive colloidal systems from mixed brush-coated nanoparticles. Adv Funct Mater. 2007;17:2307–2314.
[60] Ohno K, Morinaga T, Koh K, et al. Synthesis of monodisperse silica particles coated with well-defined, high-density polymer brushes by surface-initiated atom transfer radical polymerization. Macromolecules. 2005;38:2137–2142.
[61] Carrot G, Diamanti S, Manuszak M, et al. Atom transfer radical polymerization of n-butyl acrylate from silica nanoparticles. J Polym Sci A Polym Chem. 2001;39:4294–4301.
[62] Badrzadeh F, Akbarzadeh A, Zarghami N, et al. Comparison between effects of free curcumin and curcumin loaded NIPAAm-MAA nanoparticles on telomerase and PinX1 gene expression in lung cancer cells. Asian Pac J Cancer Prev. 2014;15:8931–8936.
[63] Nejati-Koshki K, Mesgari M, Ebrahimi E, et al. Synthesis and *in vitro* study of cisplatin-loaded Fe3O4 nanoparticles modified with PLGA-PEG6000 copolymers in treatment of lung cancer. J Microencaps. 2014;31:815–823.
[64] Reddy KR, Park W, Sin BC, et al. Synthesis of electrically conductive and superparamagnetic monodispersed iron oxide-conjugated polymer composite nanoparticles by *in situ* chemical oxidative polymerization. J Colloid Interface Sci. 2009;335:34–39.
[65] Abbasian M, Ahmadkhani L. Synthesis of conductive PSt-g-PANi/TiO2 nanocomposites by metal catalyzed and chemical oxidative polymerization. Des Monom Polym. 2016;19:585–595.
[66] Sun J, Zhou S, Hou P, et al. Synthesis and characterization of biocompatible Fe3O4 nanoparticles. J Biomed Mater Res A. 2007;80: 333–341.
[67] Wang J-S, Matyjaszewski K. Controlled/"living" radical polymerization. Atom transfer radical polymerization in the presence of transition-metal complexes. J Am Chem Soc. 1995;117:5614–5615.
[68] Coessens V, Pintauer T, Matyjaszewski K. Functional polymers by atom transfer radical polymerization. Prog Polym Sci. 2001;26: 337–377.
[69] Braunecker WA, Matyjaszewski K. Controlled/living radical polymerization: features, developments, and perspectives. Prog Polym Sci. 2007;32:93–146.